Numerical simulation of Forchheimer flow to a partially penetrating well with a mixed-type boundary condition

Simon A. Mathias [a,*], Zhang Wen [b]

[a] Department of Earth Sciences, Durham University, Durham, UK
[b] School of Environmental Studies, China University of Geosciences, Wuhan, China

SUMMARY

This article presents a numerical study to investigate the combined role of partial well penetration (PWP) and non-Darcy effects concerning the performance of groundwater production wells. A finite difference model is developed in MATLAB to solve the two-dimensional mixed-type boundary value problem associated with flow to a partially penetrating well within a cylindrical confined aquifer. Non-Darcy effects are incorporated using the Forchheimer equation. The model is verified by comparison to results from existing semi-analytical solutions concerning the same problem but assuming Darcy's law. A sensitivity analysis is presented to explore the problem of concern. For constant pressure production, Non-Darcy effects lead to a reduction in production rate, as compared to an equivalent problem solved using Darcy's law. For fully penetrating wells, this reduction in production rate becomes less significant with time. However, for partially penetrating wells, the reduction in production rate persists for much larger times. For constant production rate scenarios, the combined effect of PWP and non-Darcy flow takes the form of a constant additional drawdown term. An approximate solution for this loss term is obtained by performing linear regression on the modeling results.

© 2015 Published by Elsevier B.V.

1. Introduction

Energy losses associated with fluid production wells are often considered to comprise of three components: (1) energy losses within the aquifer as predicted by Darcy's law; (2) energy losses that occur adjacent to and within the borehole and well-screen (sometimes referred to as skin effects); and (3) non-linear energy losses associated with inertial and/or turbulent effects near the well (Konikow et al., 2009). These latter non-linear losses can be represented within numerical groundwater models using the Forchheimer equation (Mayaud et al., 2014). The Forchheimer equation is also often used to understand processes associated with oil and gas production (Huang and Ayoub, 2008; Zeng and Zhao, 2008; Wu et al., 2011) and gas injection (Mathias et al., 2009, 2014; Mijic et al., 2014).

In a recent study, Mathias and Todman (2010) demonstrated how the transient development of non-linear energy losses, associated with step drawdown tests in groundwater production wells, can be explained by invoking non-Darcy effects associated with the Forchheimer equation, using the numerical model developed by Mathias et al. (2008). However, a significant shortcoming of

the Mathias et al. (2008) model is the assumption of a fully penetrating well. In many cases, production wells only partially penetrate the aquifer of concern.

Given that non-Darcy effects are localized around areas of high flow velocities, the potentially large vertical fluxes above and below a partially penetrating well are likely to generate significant additional Non-Darcian energy losses. Wen et al. (2013, 2014) sought to explore these effects by developing a semi-analytical solution for flow to a partially penetrating well using the so-called Izbash equation. The Izbash equation assumes that flow rate is proportional to some power law of the hydraulic gradient, as opposed to Darcy's law, which assumes that flow is linearly proportional to the hydraulic gradient.

Whilst the study gave some interesting insights concerning the behavior of the Izbash equation in the presence of a partially penetrating well, their mathematical development involves imposing a number of restrictive assumptions. Firstly, it assumes that Darcy's law applies for vertical fluxes (the Izbash equation is only used for radial flow). Secondly, the Izbash equation is used as opposed to the Forchheimer equation. The Forchheimer equation is more appropriate in this context, because it is capable of recognizing that flow becomes Darcian far away from the production well. Finally, it is assumed that the water flux across the well-screen is uniform. In fact, the flux distribution across the

---

* Corresponding author. Tel.: +44 (0)1913343491; fax: +44 (0)1913342301.
  E-mail address: s.a.mathias@durham.ac.uk (S.A. Mathias).

well-screen is non-uniform, with the largest fluxes occurring at the ends of the well-screen (Mathias and Butler, 2007).

Consider production from a vertically orientated well-bore with a well-screen that is exposed to a limited thickness within a given aquifer system. The boundary condition at the well-screen is best represented as a fixed pressure condition, based on the fluid pressure within the well-bore. At the well-bore, above and below the well-screen, the boundary condition takes the form of a zero flux. Therefore there are two boundary types along the side of the well as it intersects the aquifer. Consequently, this problem is often referred to as a mixed-type boundary value problem (Cassiani et al., 1999; Chang and Chen, 2003).

Much attention has been focused on the derivation of analytical solutions for estimating drawdown in partially penetrating wells. Generally, these have used some form of integral transform in the vertical direction. Unfortunately, such a technique does not allow for the possibility of applying a mixed-type boundary condition. Therefore, the boundary at the well-screen is generally approximated using a uniform flux condition, based on the vertically averaged radial pressure gradient at the well-screen (e.g. Dougherty and Babu, 1984; Moench, 1997; Mishra and Neuman, 2011).

Perina and Lee (2006) conducted a series of studies to investigate the implications of imposing a uniform flux across the well-screen. They observed that the uniform flux assumption can lead to as much as 18% error in the estimated drawdown. The reason is that the mixed-type boundary condition gives rise to very large fluxes at the top and bottom of the well-screen. Indeed, for the extreme case of a circular plate of raised potential in a semi-infinite medium, these edge fluxes are infinite (Mathias and van Reeuwijk, 2009; Sneddon, 1966). Therefore, to better understand the nature of non-Darcy flow around a partially penetrating well, it is important to adequately incorporate this mixed-type boundary in full.

Some semi-analytical solutions have been derived for Darcian flow problems in the presence of mixed-type boundaries. These have either used dual-integral equations (Cassiani et al., 1999) or imposed a discrete non-uniform well-screen flux distribution, defined using an inverse matrix method (Chang and Chen, 2003; Perina and Lee, 2006; Mathias and Butler, 2007; Klammler et al., 2011). Such approaches are cumbersome to evaluate and employ either numerical integration methods or discretisation methods. Furthermore, they are unlikely to be amenable to non-linear problems such as those associated with the Forchheimer equation. Therefore, in this article, the relevant governing equations for Forchheimer flow to a partially penetrating well in a confined aquifer, are solved using a method of lines approach based on a finite difference spatial discretisation, similar to that used by Mathias et al. (2008).

The objective of this article is to evaluate the importance of non-Darcy energy losses during fluid production from a partially penetrating well (including for a mixed-type boundary condition representation of the well-bore boundary) in a cylindrical confined aquifer. The outline of the article is as follows: The relevant governing equations along with initial and boundary conditions are presented. These are converted to a dimensionless form similar to that previously used by Chang and Chen (2003). The numerical methods are described, in particular the grid refinement around the well-screen. The developed model is then bench-marked by comparison with the semi-analytical solutions of Cassiani et al. (1999) and Chang and Chen (2003). Non-Darcy effects are then explored in the context of constant pressure production and constant rate production.

2. Governing equations

The governing equations for fluid pressure for radially symmetric flow of water to a partially penetrating production well in a homogenous, vertically anisotropic, confined, cylindrical aquifer of radial extent, r_e [L], and thickness, H [L], can be written as follows:

$$\phi(c_w + c_r)\frac{\partial P}{\partial t} = -\frac{1}{r}\frac{\partial(rq_r)}{\partial r} - \frac{\partial q_z}{\partial z} \quad (1)$$

where ϕ [–] is porosity, c_w [M^{-1}LT^2] and c_r [M^{-1}LT^2] are the compressibilities of water and rock, respectively, P [ML^{-1}T^{-2}] is fluid pressure, t [T] is time, r [L] is radial distance from the production well, z [L] is elevation from the base of the aquifer and the volumetric fluxes, q_r [LT^{-1}] and q_z [LT^{-1}], are found from the Forchheimer (1901) equations (see Appendix A and Knupp and Lage (1995))

$$q_r = -\frac{Fk_r}{\mu_w}\frac{\partial P}{\partial r} \quad (2)$$

$$q_z = -\frac{Fk_z}{\mu_w}\frac{\partial P}{\partial z} \quad (3)$$

where F [–] is a non-Darcy factor found from

$$F = \left[1 + \frac{\rho_w}{\mu_w}\left(c_{Fr}^2 c_{Fz} k_r^2 k_z\right)^{1/3}\left(k_r^{-1}q_r^2 + k_z^{-1}q_z^2\right)^{1/2}\right]^{-1} \quad (4)$$

and μ_w [ML^{-1}T^{-1}] is the dynamic viscosity of water, ρ_w [ML^{-3}] is the density of water and k_r [L^2], k_z [L^2], c_{Fr} [–] and c_{Fz} [–] are the permeabilities and the Forchheimer inertia coefficients in the r and z direction, respectively. Note that for isotropic media, the Forchheimer inertia coefficient, c_F, can be estimated using the Geertsma (1974) correlation, $c_F = 0.005\phi^{-5.5}$.

The relevant initial and boundary conditions are as follows:

$$\begin{array}{llll}
P = P_0, & r_w \leqslant r \leqslant r_e, & 0 \leqslant z \leqslant H, & t = 0 \\
q_z = 0, & r_w \leqslant r \leqslant r_e, & z = 0, & t > 0 \\
q_z = 0, & r_w \leqslant r \leqslant r_e, & z = H, & t > 0 \\
q_r = 0, & r = r_e, & 0 \leqslant z \leqslant H, & t > 0 \\
q_r = 0, & r = r_w, & 0 \leqslant z < z_w, & t > 0 \\
P = P_w, & r = r_w, & z_w \leqslant z \leqslant z_w + L, & t > 0 \\
q_r = 0, & r = r_w, & z_w + L < z \leqslant H, & t > 0
\end{array} \quad (5)$$

where P_0 [ML^{-1}T^{-2}] is the initial pressure of the aquifer prior to pumping and r_w [L], z_w [L], L [L] and P_w [ML^{-1}T^{-2}] are the radius, elevation of base, length and fluid pressure of the well-screen associated with the production well, respectively.

The well pressure, P_w, is related to the production rate, Q [L^{3}T^{-1}], via the conservation equation (Papadopulos and Cooper, 1967):

$$\frac{\pi r_c^2}{\rho_w g}\frac{dP_w}{dt} + Q + 2\pi r_w \int_{z_w}^{z_w+L} q_r(r = r_w, z, t)dz = 0 \quad (6)$$

where r_c [L] is the radius of the well casing and g [LT^{-2}] is gravitational acceleration. It is further assumed that

$$P_w(t = 0) = P_0 \quad (7)$$

3. Dimensionless transformation

Introducing the following dimensionless transformations:

$$r_{cD} = \frac{r_c}{[\phi(c_w + c_r)\rho_w gL]^{1/2}r_w}, \quad z_{wD} = \frac{z_w}{L} \quad (8)$$

$$P_D = \frac{2\pi Lk_r(P_0 - P)}{\mu_w Q}, \quad P_{wD} = \frac{2\pi Lk_r(P_0 - P_w)}{\mu_w Q} \quad (9)$$

$$q_{rD} = -\frac{2\pi Lr_w q_r}{Q}, \quad q_{zD} = -\frac{2\pi Lr_w q_z}{Q}\left(\frac{k_r L}{k_z r_w}\right) \quad (10)$$

$$r_D = \frac{r}{r_w}, \quad z_D = \frac{z}{L}, \quad t_D = \frac{k_r t}{\mu_w \phi (c_w + c_r) r_w^2} \tag{11}$$

$$\omega = \frac{L}{H}, \quad \lambda = \left(\frac{k_r}{k_z}\right)^{1/2} \frac{L}{r_w} \tag{12}$$

$$b_D = \frac{\rho_w Q}{2\pi L k_r^{1/2} r_w \mu_w} \left(c_{Fr}^2 c_{Fz} k_r^2 k_z\right)^{1/3} \tag{13}$$

the set of equations in the previous section reduce to the following dimensionless problem:

$$\frac{\partial P_D}{\partial t_D} = -\frac{1}{r_D} \frac{\partial (r_D q_{rD})}{\partial r_D} - \frac{1}{\lambda^2} \frac{\partial q_{zD}}{\partial z_D} \tag{14}$$

$$q_{rD} = -F \frac{\partial P_D}{\partial r_D} \tag{15}$$

$$q_{zD} = -F \frac{\partial P_D}{\partial z_D} \tag{16}$$

$$F = \left[1 + b_D \left(q_{rD}^2 + \lambda^{-2} q_{zD}^2\right)^{1/2}\right]^{-1} \tag{17}$$

$$
\begin{array}{llll}
P_D = 0, & 1 \leqslant r_D \leqslant r_{eD}, & 0 \leqslant z_D \leqslant \omega^{-1}, & t_D = 0 \\
q_{zD} = 0, & 1 \leqslant r_D \leqslant r_{eD}, & z_D = 0, & t_D > 0 \\
q_{zD} = 0, & 1 \leqslant r_D \leqslant r_{eD}, & z_D = \omega^{-1}, & t_D > 0 \\
q_{rD} = 0, & r_D = r_{eD}, & 0 \leqslant z_D \leqslant \omega^{-1}, & t_D > 0 \\
q_{rD} = 0, & r_D = 1, & 0 \leqslant z_D < z_{wD}, & t_D > 0 \\
P_D = P_{wD}, & r_D = 1, & z_{wD} \leqslant z_D \leqslant z_{wD} + 1, & t_D > 0 \\
q_{rD} = 0, & r_D = 1, & z_{wD} + 1 < z_D \leqslant \omega^{-1}, & t_D > 0
\end{array}
\tag{18}
$$

$$\frac{r_{cD}^2}{2} \frac{dP_{wD}}{dt_D} - 1 + \int_{z_{wD}}^{z_{wD}+1} q_{rD}(r_D = r_{wD}) dz_D = 0 \tag{19}$$

$$P_{wD}(t_D = 0) = 0 \tag{20}$$

4. Writing the non-Darcy factor in terms of pressure gradients

It is useful to write the expression for the non-Darcy factor given in Eq. (17) in terms of pressure gradients as opposed to fluxes. Note that substituting Eqs. (15) and (16) into Eq. (17) leads to

$$F = \frac{1}{1 + b_D F J} \tag{21}$$

where

$$J = \left[\left(\frac{\partial P_D}{\partial r_D}\right)^2 + \frac{1}{\lambda^2} \left(\frac{\partial P_D}{\partial z_D}\right)^2\right]^{1/2} \tag{22}$$

Given that J is always positive, the positive root of Eq. (21) can be written as

$$F = \frac{(1 + 4b_D J)^{1/2} - 1}{2 b_D J} \tag{23}$$

A disadvantage of the above equation is that it becomes difficult to evaluate for the small pressure gradients (i.e. small J) that are expected far away from the well. However, if we multiply the top and bottom of Eq. (23) by $[(1 + 4b_D J)^{1/2} + 1]$, it can be seen that (Mathias et al., 2014)

$$F = \frac{2}{1 + (1 + 4b_D J)^{1/2}} \tag{24}$$

which is much more convenient in this context.

5. Numerical solution

Following Mathias et al. (2008), numerical solution of the above set of equations is achieved by discretising in space, using finite difference approximations, and solving the resulting set of coupled ordinary differential equations using MATLAB's ode solver, ODE15s. ODE15s uses adaptive time-stepping to ensure numerical error remains below a pre-defined tolerance, therefore time-steps are not specified a priori.
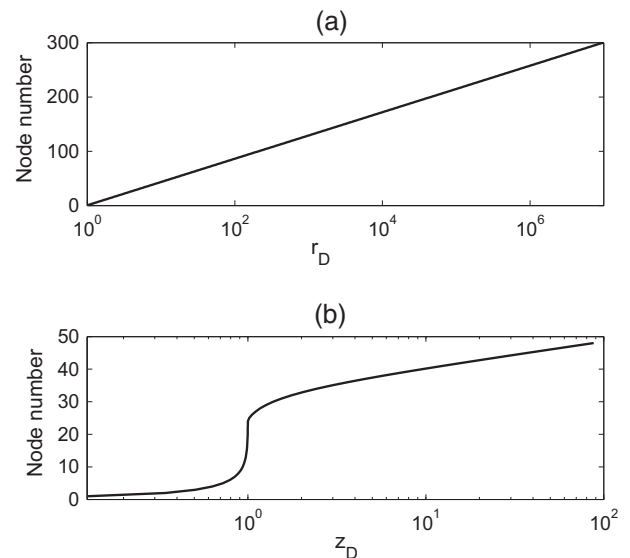
Pressure gradients are highest around the production well and then decrease ultimately to zero at the far-field boundaries. Therefore, the location of discretisation points in the radial direction are logarithmically spaced such that finer resolution is provided around the production well.

Special care must be taken to ensure adequate vertical grid resolution is provided around the locations of boundary-type changes, as these have a tendency of yielding exceptionally high gradients in their near vicinity (Mathias and Butler, 2007; Mathias and van Reeuwijk, 2009). Following Chang and Chen (2003), z_{wD} is set to zero. Therefore, a high level of vertical discretisation is only required immediately above and immediately below $z_D = 1$. Locations of the discretisation points in the vertical direction are chosen such that they are logarithmically spaced above and below $z_D = 1$, with the finer spaced points clustered around $z_D = 1$. For illustrative purposes, the locations of the finite difference nodes, in both the r_D and z_D directions, used for a simulation with $r_{eD} = 10^7$ and $\omega = 0.01$, are shown in Fig. 1.
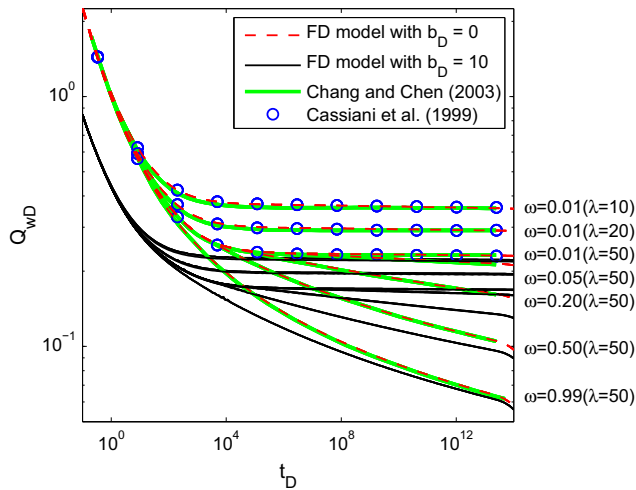
The integration associated with the integral term in Eq. (19) is evaluated using trapezoidal integration.

6. Simulations assuming a constant well pressure

Before using the numerical model to investigate the effects of Non-Darcy flow around a partially penetrating well, it is important to verify that the model predicts the same results as the semi-analytical solution of Chang and Chen (2003) when b_D is set to zero. Chang and Chen (2003) considered an identical scenario as described above except that they only looked at when $b_D = 0$ and also fixed $P_{wD} = 1$. They then used their semi-analytical solution

Fig. 1. Illustration of the spatial discretisation used for the scenario with $r_{eD} = 10^7$ and $\omega = 0.01$. (a) Plot of dimensionless radial distance, r_D, against node number. (b) Plot of dimensionless vertical distance, z_D, against node number.

Fig. 2. Plot of dimensionless production rate, Q_{wD}, against dimensionless time, t_D, for the range of constant well pressure scenarios previously studied by Chang and Chen (2003). Values of ω and λ assumed are displayed in the text-labels to the right-hand-side of the figure. The red dashed lines were obtained using the finite difference (FD) model with b_D set to zero. The black solid lines were obtained using the finite difference model with $b_D = 10$. The green solid lines were obtained using the semi-analytical solution of Chang and Chen (2003). The blue circular markers were obtained using the semi-analytical solution of Cassiani et al. (1999), which assumes that $\omega = 0$. (For interpretation of the references to color in this figure legend, the reader is referred to the web version of this article.)
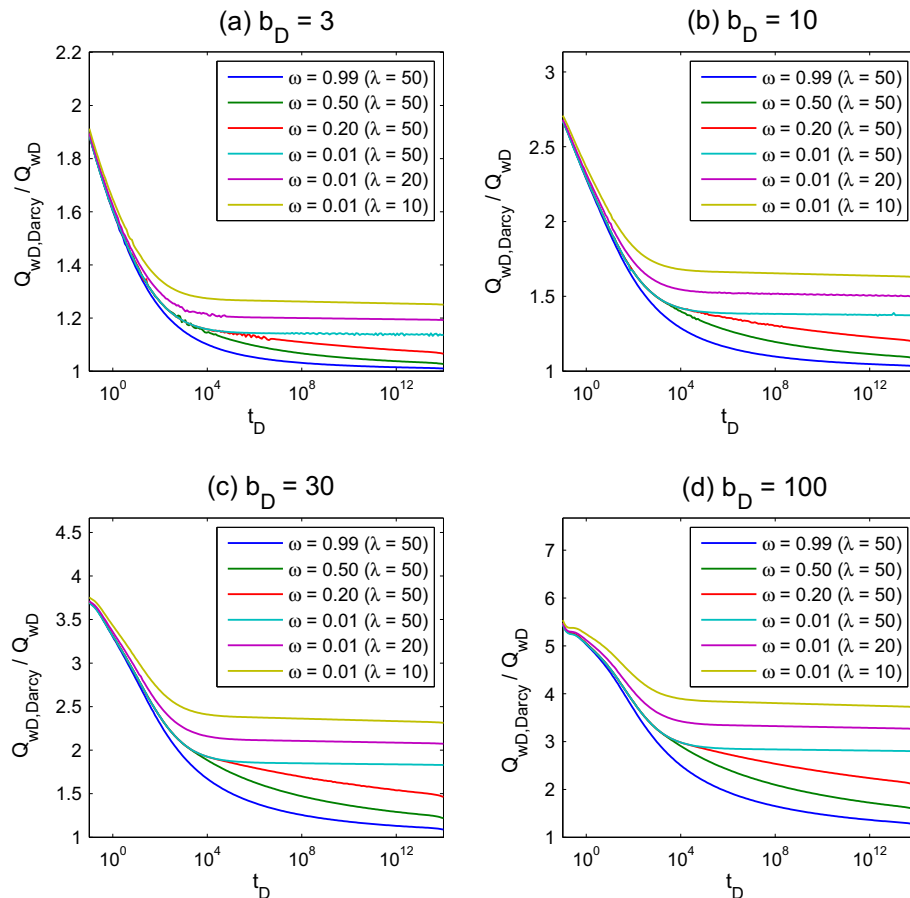
to calculate the dimensionless production rate at the well-screen, Q_{wD}, which can be found from

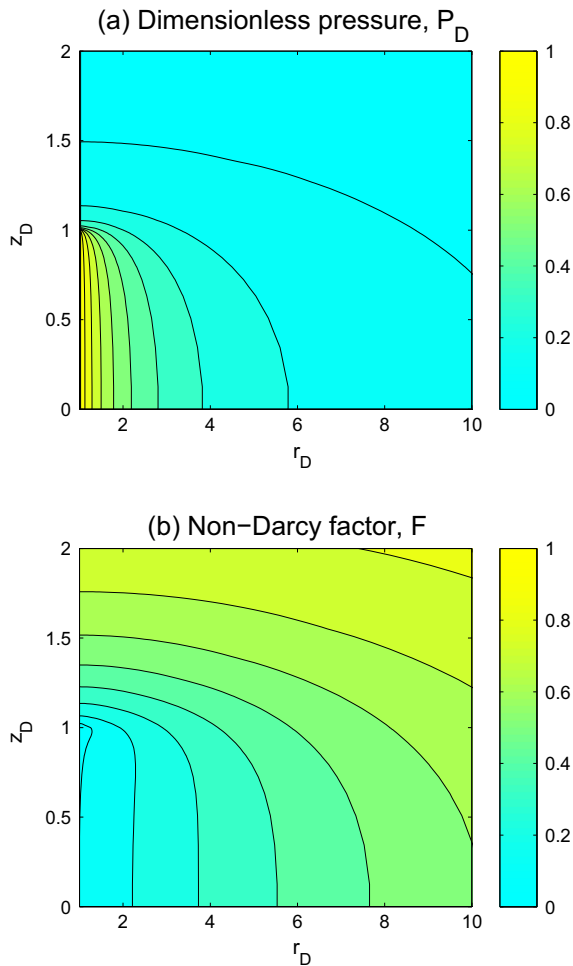$$Q_{wD} = \int_{z_{wD}}^{z_{wD}+1} q_{rD}(r_D = r_{wD})dz_D \tag{25}$$

The semi-analytical solution of Chang and Chen (2003) involved Laplace transforming the time dimension and then Fourier cosine transforming the vertical dimension. The resulting set of ordinary differential equations were then solved to obtain analytical solutions in terms of modified Bessel functions. The non-uniform well flux was imposed by discretising the well-screen and superimposing a sequence of discrete production rates, obtained using an inverse matrix method. The resulting set of equations were inverted back to the time-domain using a numerical inverse Laplace transform algorithm.

Chang and Chen (2003) reports the time-series of Q_{wD} for a range of different combinations of λ and ω. The results from Chang and Chen (2003) are shown as green lines in Fig. 2. Results from our finite difference model with $b_D = 0$ are shown as red dashed lines. It can be seen that the correspondence between the two models is excellent. However, note that just before $t_D = 10^{14}$, Q_{wD} from the finite difference model starts to drop a little below the trajectory predicted by Chang and Chen (2003). This is due to the pressure perturbation finally hitting the impermeable boundary at $r_D = r_{eD}$. Note that for all the simulations reported in this article, r_{eD} was set to 10^7.

Also shown in circular blue markers, are equivalent results from the semi-analytical solution of Cassiani et al. (1999). The conceptu-

Fig. 3. Plot of non-Darcy production rate reduction factors against dimensionless time for the constant well pressure scenarios presented in Fig. 2 for a range of different b_D values. The values of λ and ω are indicated in the legends. The values of b_D adopted are as shown in the subplot titles.

(a) Dimensionless pressure, P_D

(b) Non−Darcy factor, F

Fig. 4. Spatial distributions around the production well at $t_D = 10^{14}$ for the constant well pressure scenario with $\omega = 0.01, \lambda = 10$ and $b_D = 10$. (a) Dimensionless pressure, P_D. (b) Non-Darcy factor, F, as calculated from Eq. (24).
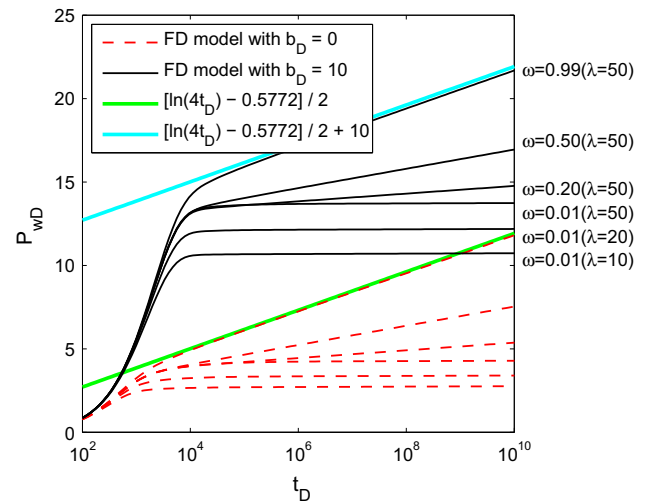
Table 1
An example of how r_{cD}, ω, λ and b_D vary with L for a practical scenario where $r_w = r_c = 0.1$ m, $\rho_w = 1000$ kg/m^3, $\mu_w = 10^{-3}$ Pa s, $k_r = 10^{-11}$ m^2, $k_z = 10^{-12}$ m^2, $\phi = 0.1, c_w = 3 \times 10^{-10}$ Pa^{-1}, $c_r = 4.5 \times 10^{-10}$ Pa^{-1}, $g = 9.81$ m/s^2, $H = 100$ m and $Q = 0.03$ m^3/s. Note that this assumes that $c_{Fr} = c_{Fz} = c_F$ where c_F is obtained from the Geertsma (1974) correlation ($c_F = 0.005\phi^{-5.5}$).

L (m)	10	20	30
r_{cD} (−)	369	261	213
ω (−)	0.1	0.2	0.3
λ (−)	316	632	949
b_D (−)	11.08	5.54	3.69

al model adopted by Cassiani et al. (1999) is identical to that of Chang and Chen (2003) except that they considered a semi-infinite aquifer such that $\omega \rightarrow 0$. The solution procedure involved the so-called dual-integral integration method, and did not involve the need to discretise the well-screen. Again, it can be said there is very good correspondence between the Cassiani et al. (1999) work and the response from the finite difference model when $\omega = 0.01$.

The black solid lines shown in Fig. 2 are from the finite difference model with exactly the same setup except that b_D was set to 10. Therefore, this model represents a non-Darcian deviation from the work of Chang and Chen (2003). It can be seen that during early times ($t_D < 10$), the production rate is less than half of the
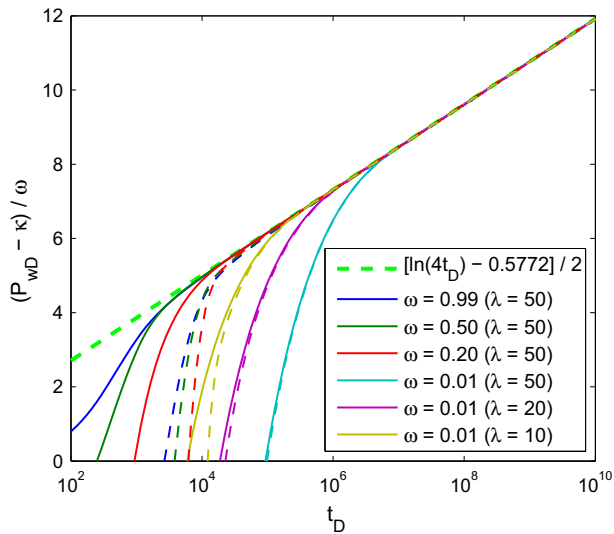

Fig. 5. Plot of dimensionless well pressure, P_{wD}, against dimensionless time, t_D, assuming a constant production rate, as described in Eq. (19), for the ω and λ scenarios used in the constant pressure study of Chang and Chen (2003) (as indicated in the text labels to the right-hand-side of the plot). The red dashed lines are due to the finite difference (FD) model with $b_D = 0$. The black solid lines are for a similar set of simulations but with $b_D = 10$. The green line is due to the (Cooper and Jacob, 1946) equation (Eq. (26) with $b_D = 0$). The cyan line is the Jacob equation with incorporation of the Forchheimer effects, as derived by Mathias et al. (2008) (Eq. (26)). (For interpretation of the references to color in this figure legend, the reader is referred to the web version of this article.)

rate generated by the Darcian models, for all values of ω. At later times ($t_D > 10^{12}$), for the case of a (close to) fully penetrating well (i.e., $\omega = 0.99$), the non-Darcian and Darcian models converge. Similar findings were also reported from the one-dimensional flow (as opposed to radial flow) simulations, also undertaken using the Forchheimer equation, previously presented by Moutsopoulos and Tsihrintzis (2005). However, Fig. 2 shows that as the production well becomes smaller, relative to the formation thickness, the non-Darcian model produces progressively less fluid than the corresponding Darcian system where $b_D = 0$, regardless of the time considered.

To explore these effects further, the simulations presented in Fig. 2 were repeated for a range of different b_D values. Fig. 3 shows plots of the ratio of Q_{wD} from the Darcian model (i.e., with $b_D = 0$), denoted $Q_{wD,Darcy}$, to the Q_{wD} calculated from the non-Darcian models against dimensionless time. This ratio represents the transient production rate reduction factor due to non-Darcy effects.

In Fig. 3a, it can be seen that when $b_D = 3$, for dimensionless times greater than 10^4, the non-Darcy effects represent less than a factor of 1.3, regardless of the values of ω and λ assigned. However, these effects become much larger with increasing b_D. Fig. 3d shows the results when $b_D = 100$. Here it can be seen that non-Darcy effects become more significant with reducing ω and λ. Reducing ω implies that the well-screen is becoming smaller relative to the formation thickness. Reducing λ implies that the well-screen is becoming smaller relative to the well radius and/or the radial permeability is becoming less relative to the vertical permeability.

As hypothesized in the introduction, the large fluxes that develop at the top and bottom of the well-screen are found to enhance non-Darcy effects on production rates, associated with the use of the Forchheimer equation. Fig. 4a and b show the spatial distribution, at $t_D = 10^{14}$, of dimensionless pressure, P_D, and the non-Darcy factor, F (as defined in Eq. (24)), respectively, for the case when $\omega = 0.01, \lambda = 10$ and $b_D = 10$. Note from Fig. 4a that the highest pressure gradients are around the top of the well-screen at
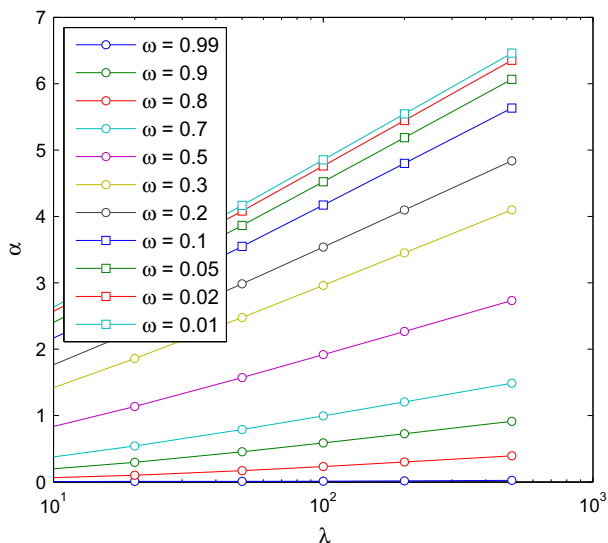
Fig. 6. Plot of $(P_{wD} - \kappa)/\omega$ against dimensionless time, t_D, for the scenarios presented in Fig. 5. Values of κ were obtained using Eq. (28). Solid and dashed lines are used for simulations with $b_D = 0$ and $b_D = 10$, respectively. The different colors are used for the different ω and λ combinations, as indicated in the legend. The Cooper and Jacob (1946) equation is also plotted, for comparison purposes, as a dashed green line. (For interpretation of the references to color in this figure legend, the reader is referred to the web version of this article.)

$z_D = 1$. In Fig. 4b it can be seen that F is significantly reduced (indicating enhanced reductions in flow due to non-Darcy effects) across the entire well-screen and, in particular, around the top of the well-screen at $z_D = 1$.

7. Simulations assuming a constant production rate

To better understand the role of partial penetration effects on step drawdown tests, it is more useful to consider a constant production rate by imposing Eq. (19). Note that r_{cD} was set to 200 for all simulations, which is a realistic value (consider Table 1) and also small enough not to significantly affect the results during the times of interest. As with the previous simulations, r_{eD} was set to 10^7 for all the simulations. Fig. 5 shows the plots of dimensionless well pressure, P_{wD}, against dimensionless time, t_D, for the

range of ω and λ adopted by Chang and Chen (2003) when studying the constant well pressure scenario. The red dashed lines are due to simulations assuming $b_D = 0$ (i.e., Darcian flow). The black solid lines are due to similar simulations but with b_D set to 10.

All the finite difference simulations are found to share a similar early time response (for $t_D < 10^2$). In this region, the system is mostly controlled by the dynamics of the well-bore equation (Eq. (19)). For $t_D > 10^3$, the simulated responses for the various combinations of ω, λ and b_D values, diverge. Nevertheless, the late time pressure responses, for all the scenarios studied, are straight-lines on a linear-log axes. The rate of dimensionless pressure increase with dimensionless time can be seen to reduce with reducing ω. Reducing ω corresponds to the well-screen becoming smaller as compared to the formation thickness. For the smallest well-screens ($\omega = 0.01$), the well pressure quickly approaches a quasi-steady-state.

Raising b_D from zero to 10 leads to an increase in well pressures for all scenarios. However, the slopes of the later time pressure responses on the linear-log axes are the same as those of their Darcian counterparts. It is also apparent that the pressure increase, due to the non-Darcy effects, decreases with reducing ω and reducing λ.

For a fully penetrating well, the late time well pressure response can be found from (Mathias et al., 2008)

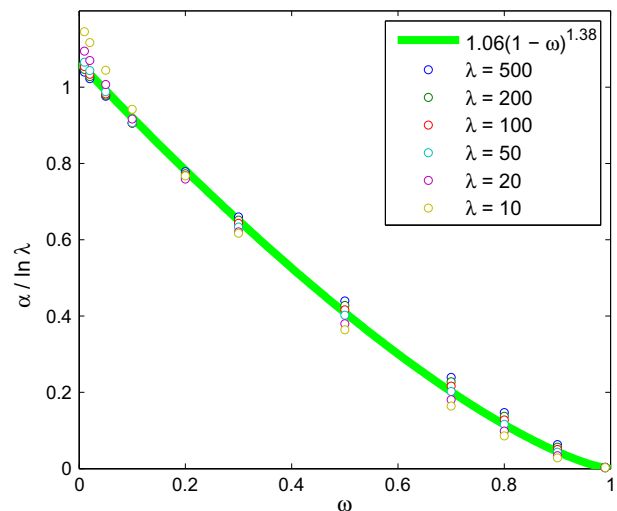$$P_{wD} = \frac{1}{2}[\ln(4t_D) - 0.5772] + b_D \tag{26}$$

which, when $b_D = 0$, reduces to the Cooper and Jacob (1946) late time response of the Theis (1935) solution. The response of Eq. (26) is shown in Fig. 5 for $b_D = 0$ and $b_D = 10$ as green and cyan solid lines, respectively. It can be seen there is a close correspondence between Eq. (26) and the finite difference models assuming $\omega = 0.99$.

To better understand how partial well penetration (PWP) influences non-Darcian losses in the well pressure, a large sensitivity analysis was performed, whereby the simulations presented in Fig. 2 were repeated for all combinations of the following parameter values:

$$\omega = [0.99 \quad 0.9 \quad 0.8 \quad 0.7 \quad 0.5 \quad 0.3 \quad 0.2 \quad 0.1 \quad 0.05 \quad 0.02 \quad 0.01]$$

$$\lambda = [500 \quad 200 \quad 100 \quad 50 \quad 20 \quad 10]$$

$$b_D = [0 \quad 1 \quad 3 \quad 10 \quad 30 \quad 100]$$

Fig. 7. Plot of α (refer to Eq. (27)) against λ for all values of ω studied. Note that α is independent of b_D.

Fig. 8. Plot of $\alpha/\ln\lambda$ (refer to Eq. (27)) against ω for all values of λ studied. Note that α is independent of b_D.
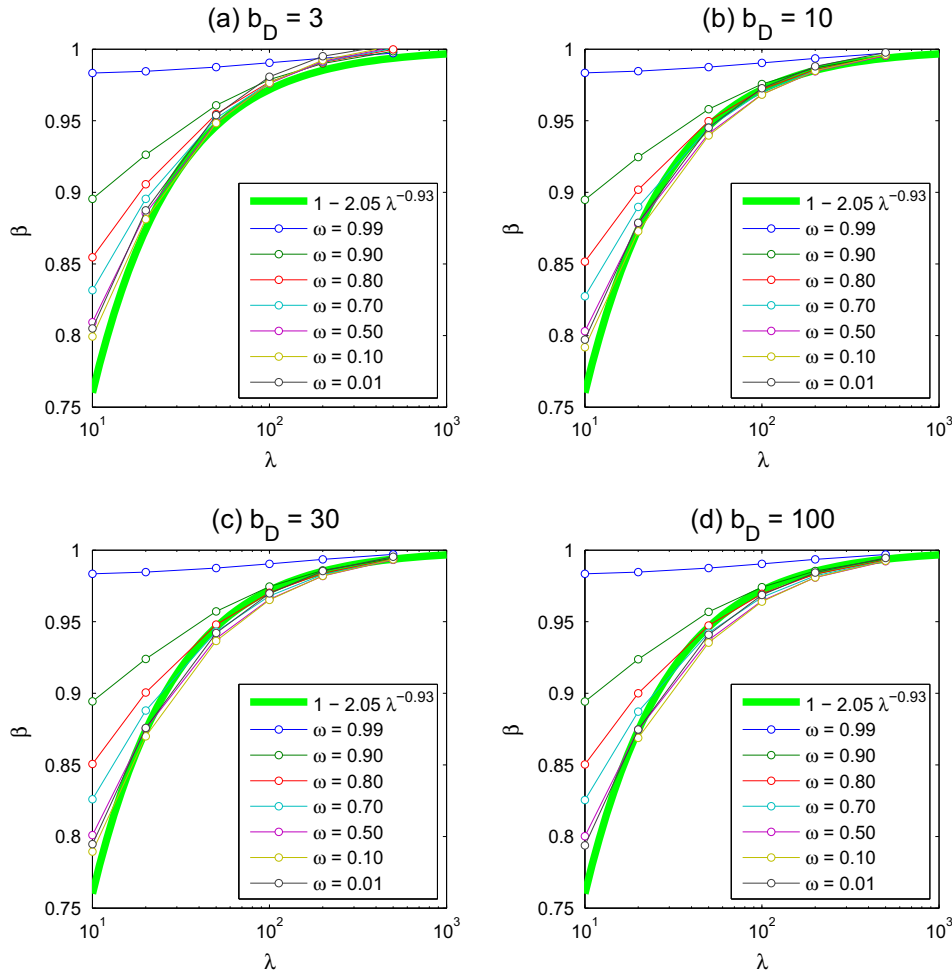
Fig. 9. Plot of β (refer to Eq. (27)) against λ for the ω values as indicated in the legend. The values of b_D adopted are as shown in the subplot titles.

For reference, Table 1 shows how these parameters vary for three different practical scenarios.

By studying the well pressures generated by the simulations and considering Eq. (26) of this article along with Eq. (44) of Chang and Chen (2003), it can be determined that the late-time response of the well-pressure takes the form

$$P_{wD} \approx \frac{\omega}{2}[\ln(4t_D) - 0.5772] + \alpha + \beta b_D \qquad (27)$$

where $\alpha = f(\omega, \lambda)$ and $\beta = f(\omega, \lambda, b_D)$.

Considering Eq. (26), a value for the bulk term, $\kappa = \alpha + \beta b_D$ can be determined for each of the simulations from

$$\kappa = P_{wD}(t_D = 10^{10}) - \frac{\omega}{2}\left[\ln(4^{10}) - 0.5772\right] \qquad (28)$$

Note that $\kappa = \alpha$ for the simulations where b_D is set to zero. Once values of α are obtained, β can be calculated by considering that $\beta = (\kappa - \alpha)/b_D$.

As an illustrative example, Fig. 6 shows a plot of $(P_{wD} - \kappa)/\omega$ (from the finite difference results) against dimensionless time, t_D, for the same scenarios presented in Fig. 5. Solid lines are used for the Darcian simulations (with $b_D = 0$) and dashed lines are used for the non-Darcian simulations (with $b_D = 10$). Values of κ were obtained using Eq. (28). It can be seen that for late times, all the finite difference simulations converge onto the Cooper and Jacob (1946) equation (i.e., Eq. (26) with $b_D = 0$), which is plotted as a dashed green line.

Fig. 7 shows plots of α against λ for all the values of ω studied. It can be seen that α increases linearly with $\ln \lambda$. The rate of increase decreases with increasing ω. For $\omega = 0.99$, α is close to zero, which is indicative of this scenario being close to a fully penetrating well. The fact that α increases with increasing λ for a given ω suggests that energy losses associated with PWP increase with decreasing well-radii.

Considering the logarithmic response of α with λ seen in Fig. 7, it is interesting to observe the plot of $\alpha/\ln\lambda$ against ω, for all λ values studied, shown in Fig. 8. Here it can be seen that all the results follow a very similar curve. A power law, fitted to the data using linear regression, is also shown for comparison as a green[1] line. The results suggest that a reasonable approximation for α can be obtained from

$$\alpha \approx 1.06(1 - \omega)^{1.38}\ln \lambda \qquad (29)$$

Plots of β against λ are presented in Fig. 9 for a range of ω and b_D values. The first thing of note is that for all the simulations, β increases with increasing λ up to maximum value of 1.0. Furthermore, it is apparent that $\beta \approx 1.0$ when $\lambda > 10^3$ for all the scenarios studied. The reason is that as λ becomes sufficiently large, the vertical gradient term in the conservation equation, Eq. (14), becomes negligibly small compared to the radial gradient term.

---

[1] For interpretation of color in Fig. 8, the reader is referred to the web version of this article.

A second point of interest is that, for $\omega \leqslant 0.7$, the relationship between β and λ converges to a single curve for all values of ω (where $\omega \leqslant 0.7$) and b_D. The reason for the β results converging on to a single curve for $\omega \leqslant 0.7$ is that, for these simulations, the non-Darcy effects are unable to propagate out to the upper boundary of the model, $z_D = \omega^{-1}$, and hence are unaffected by ω (also consider again Fig. 4b).

Applying linear regression to all values where $\omega \leqslant 0.7$ and $b_D \geqslant 10$, it was found that a reasonable approximation for β and λ can be obtained from

$$\beta \approx 1 - 2.05\lambda^{-0.93}, \quad \omega \leqslant 0.7 \tag{30}$$

Note that this approximation is also reasonable for $b_D < 10$. However, the results from the simulations undertaken with $b_D < 10$ were excluded from the regression analysis because of precision issues associated with the fact that the Non-Darcian losses associated with these simulations were smaller.

A common approach to interpreting step-drawdown tests is to analyze the resulting data using the so-called Jacob (1946) equation

$$s_w = AQ + BQ^2 \tag{31}$$

where s_w [L] is the drawdown of the water level in the production well and A [L^{-2}T] and B [L^{-5}T^2] are referred to as the formation-loss and well-loss coefficients, respectively.

The drawdown, s_w, is related to the dimensionless well pressure, P_{wD}, by

$$s_w = \frac{\mu_w Q P_{wD}}{2\pi L k_r \rho_w g} \tag{32}$$

and therefore, from Eq. (27), it can be said that

$$s_w \approx \frac{\mu_w Q}{4\pi H k_r \rho_w g} \left[\ln(4t_D) - 0.5772 + \frac{2\alpha}{\omega} \right]$$
$$+ \frac{\beta \left(c_{Fr}^2 c_{Fz} k_r^2 k_z \right)^{1/3} Q^2}{(2\pi L)^2 k_r^{3/2} r_w g} \tag{33}$$

Comparing this with Eq. (31), it can be seen that the well-loss coefficient can be calculated from

$$B = \frac{\beta \left(c_{Fr}^2 c_{Fz} k_r^2 k_z \right)^{1/3}}{(2\pi L)^2 k_r^{3/2} r_w g} \tag{34}$$

from which it can be seen that the non-Darcian well-loss coefficient, B, is inversely proportional to the square of the well-screen length, L.

8. Summary and conclusions

The objective of this study was to investigate the role of partial well penetration (PWP) on non-Darcian well losses associated with groundwater production wells. A numerical finite difference model, for solving the problem of Forchheimer flow to a partially penetrating well, was developed in MATLAB for this purpose. Special attention was made to provide sufficient grid-resolution around the top of the well-screen, so as to adequately capture the large fluxes that develop as a consequence of the mixed type boundary condition at the well-bore. The model was verified by comparison with the semi-analytical solutions of Chang and Chen (2003) and Cassiani et al. (1999), which solve for the problem of Darcian flow to a partially penetrating well.

Normalizing the governing equations to a set of dimensionless variables revealed that there were just three parameter groups of interest: (1) the ratio of well-screen length to formation thickness, ω; (2) the ratio of well-screen length to well radius, λ; and (3) a normalized parameter group containing the product of the Forchheimer parameter and the production rate, b_D.

The model was first implemented to explore the combined role of PWP and non-Darcy effects on the decline in production rate associated with constant pressure boundary conditions at the well-screen. Non-Darcy effects lead to a reduction in production rate in this context, as compared to an equivalent problem solved using Darcy's law. For fully penetrating wells, this reduction in production rate becomes less significant with time. However, for partially penetrating wells, the reduction in production rate persists for much larger times (recall Fig. 3).

To better understand how PWP might affect performance during a step-drawdown test, the model was implemented using a constant rate of production. A sensitivity analysis was then undertaken to explore the combined role of PWP and non-Darcy effects on well pressure development. For large times, the combined effect of PWP and non-Darcy flow takes the form of a constant additional drawdown term (recall Eq. (27)). An approximate solution for this loss term was obtained by performing linear regression on the modeling results (recall Eqs. (29) and (30)).

Appendix A. Anisotropic Forchheimer equation

From Eq. (6.3) of Knupp and Lage (1995), the Forchheimer equation for an anisotropic porous media is found to take the form

$$\left(\frac{-1}{\rho_w} \right) \nabla P = v_w \left[1 + v_w \rho_w \Gamma \kappa (\mathbf{q} \cdot \mathbf{k}^{-1} \mathbf{q})^{1/2} \right] \mathbf{k}^{-1} \mathbf{q} \tag{A.1}$$

where $\Gamma = (\det \gamma)^{1/3}$ with $\gamma = \mathbf{c_F}/(v_w^2 \rho_w)$ (see paragraph preceding Eq. (6.1) in Knupp and Lage (1995)), $\kappa = (\det \mathbf{k})^{1/3}$ (see paragraph preceding Eq. (5.3) in Knupp and Lage (1995)), $\mathbf{q}$ [LT^{-1}] is a vector of volumetric fluxes and $\mathbf{c_F}$ [–] and $\mathbf{k}$ [L^2] are the tensors for the Forchheimer inertia coefficient and permeability, respectively.

Noting that v_w is the kinematic viscosity, found from $v_w = \mu_w/\rho_w$, Eq. (A.1) can be rearranged to obtain

$$\mathbf{q} = -\frac{F\mathbf{k}}{\mu_w} \nabla P \tag{A.2}$$

where

$$F = \left[1 + \frac{\rho_w}{\mu_w} (\det \mathbf{c_F} \det \mathbf{k})^{1/3} \left(\mathbf{q} \cdot \mathbf{k}^{-1} \mathbf{q} \right)^{1/2} \right]^{-1} \tag{A.3}$$

When the principle axes of anisotropy are aligned with the geometrical axes under consideration, the tensors simplify such that

$$\mathbf{c_F} = \begin{bmatrix} c_{Fx} & 0 & 0 \\ 0 & c_{Fy} & 0 \\ 0 & 0 & c_{Fz} \end{bmatrix} \tag{A.4}$$

and

$$\mathbf{k} = \begin{bmatrix} k_x & 0 & 0 \\ 0 & k_y & 0 \\ 0 & 0 & k_z \end{bmatrix} \tag{A.5}$$

and consequently, Eq. (A.3) reduces to

$$F = \left[1 + \frac{\rho_w}{\mu_w}\left(c_{Fx}c_{Fy}c_{Fz}k_xk_yk_z\right)^{1/3}\left(k_x^{-1}q_x^2 + k_y^{-1}q_y^2 + k_z^{-1}q_z^2\right)^{1/2}\right]^{-1}$$

(A.6)

where $c_{Fx}, c_{Fy}, c_{Fz}, k_x, k_y, k_z, q_x, q_y$ and q_z are the Forchheimer inertia coefficients, permeabilities and volumetric fluxes in the x, y and z direction, respectively.

For the axially symmetric problem of interest in this article, $c_{Fx} = c_{Fy} = c_{Fr}, k_x = k_y = k_r$ and $q_r^2 = q_x^2 + q_y^2$, where c_{Fr} and k_r are the Forchheimer inertia coefficient and permeability in the r direction. Consequently, Eq. (A.6) reduces further to

$$F = \left[1 + \frac{\rho_w}{\mu_w}\left(c_{Fr}^2 c_{Fz}k_r^2 k_z\right)^{1/3}\left(k_r^{-1}q_r^2 + k_z^{-1}q_z^2\right)^{1/2}\right]^{-1}$$

(A.7)

References

Cassiani, G., Kabala, Z.J., Medina Jr., M.A., 1999. Flowing partially penetrating well: solution to a mixed-type boundary value problem. Adv. Water Resour. 23, 59–68.

Chang, C.C., Chen, C.S., 2003. A flowing partially penetrating well in a finite-thickness aquifer: a mixed-type initial boundary value problem. J. Hydrol. 271, 101–118.

Cooper, H.H., Jacob, C.E., 1946. A generalized graphical method for evaluating formation constants and summarizing well field history. Trans. Am. Geophys. Union 27, 526–534.

Dougherty, D.E., Babu, D.K., 1984. Flow to a partially penetrating well in a double-porosity reservoir. Water Resour. Res. 20, 1116–1122.

Forchheimer, P., 1901. Wasserbewegung durch Boden. Z. Ver. Deutsch. Ing. 45, 1782–1788.

Geertsma, J., 1974. Estimating the coefficient of inertial resistance in fluid flow through porous media. SPE J., 445–450 (SPE Paper No 4706).

Huang, H., Ayoub, J.A., 2008. Applicability of the Forchheimer equation for non-Darcy flow in porous media. SPE J. 13, 112–122.

Jacob, C.E., 1946. Drawdown test to determine effective radius of artesian well. Proc. ASCE 72, 629–646.

Klammler, H., Hatfield, K., Nemer, B., Mathias, S.A., 2011. A trigonometric interpolation approach to mixed-type boundary problems associated with permeameter shape factors. Water Resour. Res. 47, W03510.

Knupp, P.M., Lage, J.L., 1995. Generalization of the Forchhimer-extended Darcy flow model to the tensor permeability case via a variational principle. J. Fluid Mech. 299, 97–104.

Konikow, L.F., Hornberger, G.Z., Halford, K.J., Hanson, R.T., 2009. Revised multi-node well (MNW2) package for MODFLOW ground-water flow model, U.S. Geological Survey Techniques and Methods 6A30, 67p.

Mathias, S.A., Butler, A.P., 2007. Shape factors for constant-head double-packer permeameters. Water Resour. Res. 43, W06430.

Mathias, S.A., Todman, L.C., 2010. Step-drawdown tests and the Forchheimer equation. Water Resour. Res. 46, W07514.

Mathias, S.A., van Reeuwijk, M., 2009. Hydraulic fracture propagation with 3-D leak-off. Transp. Porous Med. 80, 499–518.

Mathias, S.A., Butler, A.P., Zhan, H., 2008. Approximate solutions for Forchheimer flow to a well. J. Hydraul. Eng. 134, 1318–1325.

Mathias, S.A., Hardisty, P.E., Trudell, M.R., Zimmerman, R.W., 2009. Approximate solutions for pressure buildup during CO2 injection in brine aquifers. Transp. Porous Med. 79, 265–284.

Mathias, S.A., McElwaine, J.N., Gluyas, J.G., 2014. Heat transport and pressure buildup during carbon dioxide injection into depleted gas reservoirs. J. Fluid Mech. 756, 89–109.

Mayaud, C., Walker, P., Hergarten, S., Birk, S., 2014. Nonlinear flow process: a new package to compute nonlinear flow in MODFLOW. Groundwater. http://dx.doi.org/10.1111/gwat.12243.

Mijic, A., LaForce, T.C., Muggeridge, A.H., 2014. CO2 injectivity in saline aquifers: the impact of non-Darcy flow, phase miscibility, and gas compressibility. Water Resour. Res. 50, 4163–4185.

Mishra, P.K., Neuman, S.P., 2011. Saturated-unsaturated flow to a well with storage in a compressible unconfined aquifer. Water Resour. Res. 47, W05553.

Moench, A.F., 1997. Flow to a well of finite diameter in a homogeneous, anisotropic water table aquifer. Water Resour. Res. 33, 1397–1407.

Moutsopoulos, K.N., Tsihrintzis, V.A., 2005. Approximate analytical solutions of the Forchheimer equation. J. Hydrol. 309, 93–103.

Papadopulos, I.S., Cooper, H.H., 1967. Drawdown in a well of large diameter. Water Resour. Res. 3, 241–244.

Perina, T., Lee, T.C., 2006. General well function for pumping from a confined, leaky, or unconfined aquifer. J. Hydrol. 317, 239–260.

Sneddon, I.N., 1966. Mixed Boundary Value Problems in Potential Theory. Wiley, New York.

Theis, C.V., 1935. The relationship between the lowering of the piezometric surface and the rate and duration of discharge of a well using ground water storage. Trans. Am. Geophys. Union 16, 519–524.

Wen, Z., Liu, K., Chen, X., 2013. Approximate analytical solution for non-Darcian flow toward a partially penetrating well in a confined aquifer. J. Hydrol. 498, 124–131.

Wen, Z., Liu, K., Zhan, H., 2014. Non-Darcian flow toward a larger-diameter partially penetrating well in a confined aquifer. Environ. Earth Sci. 72, 4617–4625.

Wu, Y.S., Lai, B., Miskimins, J.L., Fakcharoenphol, P., Di, Y., 2011. Analysis of multiphase non-Darcy flow in porous media. Transp. Porous Med. 88, 205–223.

Zeng, F., Zhao, G., 2008. Semianalytical model for reservoirs with Forchheimer's non-Darcy flow. SPE Res. Eval. Eng. 11, 280–291.